(Received 8 February 2025, Accepted 23 May 2025, Scheduled 1 June 2025)

Machine Learning Assisted Long-Range Wireless Power Transfer

Likai Wang[1,#], Yuqian Wang[1,#], Shengyu Hu[1], Yunhui Li[2], Hong Chen[1], Ce Wang[1,*], and Zhiwei Guo[1,*]

[1]*MOE Key Laboratory of Advanced Micro-Structured Materials School of Physics Science and Engineering, Tongji University, Shanghai 200092, China*
[2]*Department of Electrical Engineering, Tongji University, Shanghai 201804, China*

ABSTRACT: Long-range near-field magnetic resonance wireless power transfer (WPT) technology holds broad application prospects in fields such as medical implants and industrial manufacturing robots. However, it faces challenges of low efficiency and poor robustness in long-distance transmission. This study proposes an innovative collaborative optimization approach that integrates machine learning gradient descent optimization algorithm (GDOA) with non-Hermitian topological physics to precisely regulate the coupling strength distribution, thereby realizing a highly flexible, efficient, and robust WPT system capable of anchoring transmission frequencies and accommodating an arbitrary number of resonators. Experimental results demonstrate that GDOA-optimized Su-Schrieffer-Heeger (SSH)-like topological chain achieves a transmission efficiency of 65% at the target frequency and maintains 57.9% efficiency under 30% structural perturbations, significantly outperforming the SSH chain (45.6%) and uniform chain (24.1%) in control groups. This research provides theoretical and experimental support for the design of machine learning-based topological long-range WPT systems, offering substantial practical value, particularly in medical electronic power supply and wireless industrial equipment applications.

1. INTRODUCTION

Magnetic resonance wireless power transfer (WPT) technology [1, 2] has shown great potential in various fields such as smartphones, robotics, medical implants, and electric vehicles, attracting extensive research interest [3–8]. However, in standard second-order resonant systems, the coupling strength between the transmitter and receiver decreases sharply as the transmission distance increases, leading to a significant drop in long-distance transfer efficiency [9–12]. To extend the transfer distance without sacrificing efficiency, researchers have proposed adding multiple relay coils between the transmitter and receiver, forming a uniform chain structure similar to dominoes [13–17]. However, this domino chain structure still faces numerous challenges in achieving stable and efficient long-distance WPT [18, 19]: (1) When the spacing between relay coils is too small, strong near-field coupling effects can cause significant frequency splitting, which is influenced by the spacing and number of coils, making it difficult to achieve stable WPT at a fixed operating frequency [20, 21]; (2) When the spacing between relay coils is larger, the frequency splitting caused by near-field coupling decreases, and the operating frequency can be fixed at the resonant frequency of the coils, but the transfer efficiency decreases accordingly, making it highly challenging to balance stability and efficiency in long-distance WPT; (3) In traditional domino systems [13], the magnetic field is almost uniformly distributed across all coils, resulting in a significant increase in overall energy loss (Ohmic loss); (4) As the number of relay coils increases, structural errors gradually accumulate, leading to a sharp decrease in transfer efficiency and increased fluctuations. Therefore, there is an urgent need to develop innovative technologies or methods to optimize existing technologies and achieve stable and efficient long-range WPT [22–26].

In recent years, the rapid development of artificial intelligence has greatly promoted the widespread application of machine learning algorithms in the field of physical multi-parameter optimization, like photonic structure design [27–29], evaporative cooling experiment optimization [30–32], and quantum state preparation [33–37]. In these application scenarios, the relationship between optimization parameters and target quantities is often regarded as a "black box", and neural network structures driven by reinforcement learning or active learning are commonly used to optimize target parameters. In particular, several recent studies have demonstrated the successful integration of machine learning techniques in electromagnetic WPT system optimization [38–41]. However, in specific situations, there is a clear functional relationship between parameters and target quantities, which provides the possibility for applying optimization strategies such as gradient descent or self-feedback [42].

This paper addresses the robustness bottlenecks (Challenges 3 and 4) inherent to long-distance chain-type WPT systems by proposing an innovative WPT scheme based on a gradient descent optimization algorithm (GDOA), designed to achieve optimal transmission efficiency. We conducted

* Corresponding authors: Ce Wang (21153@tongji.edu.cn); Zhiwei Guo (2014guozhiwei@tongji.edu.cn).
# Likai Wang and Yuqian Wang contributed equally to this work.

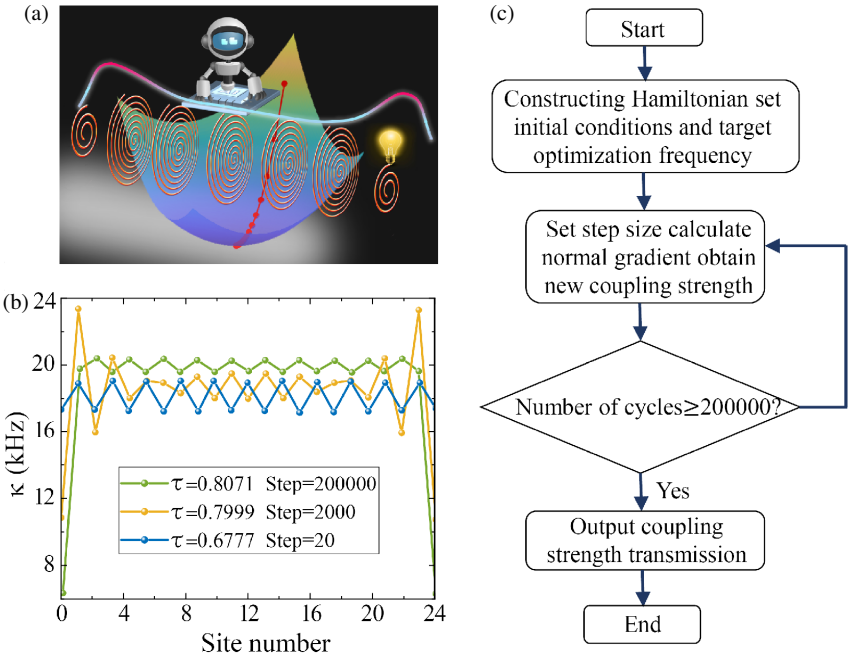

FIGURE 1. GDOA for long-range domino-like WPT system. (a) Conceptual diagram of the GDOA model. (b) Changes in efficiency and coupling distribution at training steps of 20, 2000, and 200000. The initial configuration is set to a uniform distribution, and at step 20, the GDOA extracts the SSH model. The optimized result is an improved version of the SSH model, with its coupling strengths on both sides exhibiting different characteristics compared to the traditional SSH structure. (c) Flowchart of machine learning based GDOA.

an in-depth analysis of how the coupling strength between two nearest neighbor resonant coils affects transfer efficiency and cleverly introduced GDOA for optimization. Through GDOA, we can accurately determine the specific position distribution of the resonator corresponding to the optimal transfer efficiency. To verify the effectiveness of the GDOA, we considered a second-order model with known optimal distribution exact solutions. We found that the solution provided by the GDOA is highly consistent with the exact solution and have conducted experimental verification (see Supplementary Information A [43]). Furthermore, we apply the GDOA to a high-order chain model consisting of ten oscillators. The GDOA successfully predicted the optimal model and achieved perfect impedance matching at the target frequency. Compared with traditional models such as uniform chain and SSH chain models, our optimization demonstrates significant advantages and potential in performance. This result fully demonstrates the outstanding performance of GDOA in achieving optimal transfer efficiency.

2. RESULTS

Model for long-range WPT system. Take the classical one-dimensional domino chain WPT system as an example, the dynamics at driven frequency can be described by the coupled mode theory (CMT) [44]:

$$\begin{aligned} i\frac{d\vec{a}}{dt} &= H\vec{a} + e^{-i\omega t}\sqrt{2\gamma_t}\vec{s} \\ H &= \sum_i \left[(\omega_0 - i\Gamma - i\gamma_i)c_i^\dagger c_i + \kappa_i c_{i+1}^\dagger c_i\right] + H.c. \end{aligned}, \quad (1)$$

where $c_i^\dagger(c_i)$ is the creation (annihilation) operator of the i^{th} resonator located at position r_i. For simplification, the resonant frequencies ω_0 and dissipative losses Γ of all coils are identical, and the radiative loss γ_i is nonzero only for the transmitter $\gamma_1 = \gamma_t$ and receiver $\gamma_L = \gamma_r$. The nearest-neighbor coupling strength between the i^{th} and $i+1^{\text{th}}$ coils is represented by $\kappa_i = e^{-(r_{i+1}-r_i)/d_0}$, with the normalized distance constant $d_0 = 0.0181$. $\vec{a} = (a_1, a_2, ..., a_L)^T$ is the vector representation for all the complex field a_l on the l^{th} coil, and $\vec{s} = (1, 0, ..., 0)^T$ represents the source driving on the transmitter at strength of γ_t. A straightforward calculation shows that the transmission (τ) can be given by:

$$\tau(\omega) = \left|\sqrt{2\gamma_t}a_L\right| = \left|2\sqrt{\gamma_t\gamma_r}\left(\frac{1}{H-\omega I}\right)_{L,1}\right|, \quad (2)$$

The objective function is to find the optimal $\{\kappa_l\}$ reproducing the largest $\tau(\omega)$ by adjusting the position distribution $\{r_l\}$.

GDOA. To be compact, we directly optimize $\{\kappa_l\}$ which is equivalent to the optimization of $\{r_l\}$. As illustrated in Fig. 1(a), the proposed GDOA framework employs a collaborative optimization strategy that integrates gradient descent principles with non-Hermitian topological physics. This approach enables precise regulation of coupling strength distributions across the resonator chain, ensuring robust and efficient energy transfer. We introduce the Green's function matrix as

$$G(\omega) = (H - \omega I)^{-1}. \quad (3)$$

According to Eq. (2), the transition rate is related to G as $T = \sqrt{2\gamma_t\gamma_r}\,|G_{L,1}|$. Taking the derivative of both sides of

the equation $G(H-\omega I)=I$ with respect to κ_l, we obtain

$$\frac{\partial G}{\partial \kappa_l} = -G\frac{\partial H}{\partial \kappa_l}G, \tag{4}$$

With Eq. (4), it is easy to show that

$$\frac{\partial G_{L,1}}{\partial \kappa_l} = -G_{L,l}G_{l+1,1} - G_{L,l+1}G_{l,1} \equiv \delta G_l, \tag{5}$$

as long as the real part of $\delta G_l/G_{L,1}$ is positive, an increase in the coupling κ_l can lead to a larger transition rate. Together with the constraint of $\Pi_{l=1}^{L-1}\kappa_l = T_p$, we can then introduce a gradient flow $\boldsymbol{\kappa} \to \kappa + r\Delta\boldsymbol{\kappa}$ to optimize T with

$$\Delta\boldsymbol{\kappa} = \mathrm{Re}\left(\frac{\delta \mathbf{G}}{G_{L,1}}\right) - \mathbf{T}(\boldsymbol{\kappa})\left[\mathrm{Re}\left(\frac{\delta \mathbf{G}}{G_{L,1}}\right)\cdot \mathbf{T}(\boldsymbol{\kappa})\right], \tag{6}$$

where $\mathbf{T}(\boldsymbol{\kappa}) \propto (1\kappa_1, ..., 1/\kappa_{L-1})$ is a unit vector. Following Eq. (6), we can then optimize T by repeating the gradient descent. To ensure physical consistency during optimization, it is essential to maintain the invariance of the product of coupling strengths. Therefore, we introduce a modified gradient update rule that removes components that would violate this constraint. A detailed mathematical derivation and explanation of this constraint-preserving mechanism are provided in Supplementary Information B [43]).

Figure 1(b) presents three scenarios in the training process: step sizes of 20, 2000, and 200000, when $\omega = 1\,\mathrm{kHz}$, $\gamma_0 = 0.2\,\mathrm{kHz}$, $\gamma_t = \gamma_r = 2\,\mathrm{kHz}$, and $L = 24$. Specifically, we investigate a domino-like system consisting of $L = 10$ uniformly arranged resonant units, which is used as the initial step for the GDOA. Following the flowchart shown in Fig. 1(c), iterative optimization is performed at a specific optimization operation frequency. Given the similarity between the gradient optimization chain and SSH chain, we have chosen the SSH chain as one of the comparison models, which is based on the structural characteristics observed under a very small number (≤ 20) of iterations. To further demonstrate the advantages of the GDOA over traditional optimization approaches, we compared it with commonly used methods such as Bayesian optimization and Monte Carlo simulations. Results show that GDOA achieves significantly better convergence speed and scalability. A comprehensive comparison including computational efficiency, dimensional adaptability, and accuracy is presented in Supplementary Information C [43]).

At the 30$^{\text{th}}$ iteration of the optimization process, the system's dynamic behavior demonstrates the characteristic features of the SSH model. This model, recognized for its topological robustness, ensures the stability of energy transfer by virtue of its topologically non-trivial phase. To establish a rigorous comparative research framework, the SSH model identified during the optimization process is employed as the reference benchmark for subsequent optimization analysis. For the SSH-like WPT chain, these characteristics arise from the alternating coupling strengths between adjacent resonators, which create a synthetic one-dimensional lattice with a bandgap [24]. The topology of this bandgap determines whether edge states — localized modes at the chain's ends — emerge. These states are intrinsically robust to disorder, as their existence is tied to the global symmetry of the system rather than specific local parameters.

Figure 2(a) illustrates the real part of the eigenfrequency as a function of the ratio of the strong coupling area to the weak coupling area with κ_1/κ_2 (Here we fix κ_1 to be constant at 12.78 and then change the strength of κ_2). Notably, $\kappa_1/\kappa_2 = 1$ serves as the critical point distinguishing between topologically trivial and nontrivial states. When $\kappa_1/\kappa_2 < 1$, a trivial bandgap opens near the frequency ω_0, whereas when $\kappa_1/\kappa_2 > 1$, a topologically nontrivial bandgap opens around ω_0, accompanied by the emergence of two topological edge states. Specifically, at the exceptional point $\kappa_1/\kappa_2 = 2.05$, the eigenfrequencies and eigenmodes of these two edge states coalesce. In the exact phase of parity-time-symmetry ($\kappa_1/\kappa_2 < 2.05$), the eigenfrequencies of the two edge states are purely real but deviate from ω_0. However, once entering the broken phase of parity-time-symmetry ($\kappa_1/\kappa_2 > 2.05$), the eigenfrequencies of these two edge states become complex, with the fixed real parts ω_0 (as indicated by the red solid line). It is worth noting that the remaining eight eigenfrequencies of the bulk states remain purely real throughout the phase transition (red dashed line). For details on the imaginary parts of the eigenfrequencies, please refer to the Supplementary Information D [43]. In the experimental section, we selected $\kappa_1/\kappa_2 = 1.296$ (the black dashed line), with corresponding coupling strengths and distances of $\kappa_1 = 16.58\,\mathrm{kHz}$, $d_1 = 2.5\,\mathrm{cm}$, and $\kappa_2 = 12.79\,\mathrm{kHz}$, $d_2 = 3.4\,\mathrm{cm}$. The corresponding eigenvalue distribution is shown in Fig. 2(b), where the blue dots specifically highlight the unique topological modes within the bandgap.

Furthermore, we have presented the optimization results under different conditions: Fig. 2(c) vividly illustrates the optimization scenario for the number of resonators, while Fig. 2(d) clearly demonstrates the optimization results for three different target frequencies. This fully demonstrates that our proposed novel WPT scheme can flexibly meet the optimization requirements under various objectives. Additionally, Fig. 2(e) compares the coupling coefficient κ relationship between the optimized chain (red) and the SSH chain (blue). It is evident that there are significant differences in coupling strength between the optimized chain and SSH chain, and the coupling strength of the optimized chain exhibits a symmetric distribution around the structural center (site number is 5). By calculating the wave function Ψ for both chains, we found (as shown in Fig. 2(f)) that although the intensities of the 10 resonators are similar, the wave function of the optimized chain is better localized at the ends of the structure, while the dissipation in the middle is also reduced. This indicates that, compared to the SSH chain, the optimized chain may exhibit superior robustness.

We designed three types of chains, with their coupling strengths adjusted by varying the distances. The specific parameters are as in supplementary material [43]. With other parameters kept constant, it is evident from the transmission rate versus frequency relationship shown in Fig. 3(a) that the optimized chain (red) exhibits a significantly higher transmission rate than the SSH chain (blue) and uniform chain (green). Fig. 3(b) provides a local magnification of Fig. 3(a), focusing

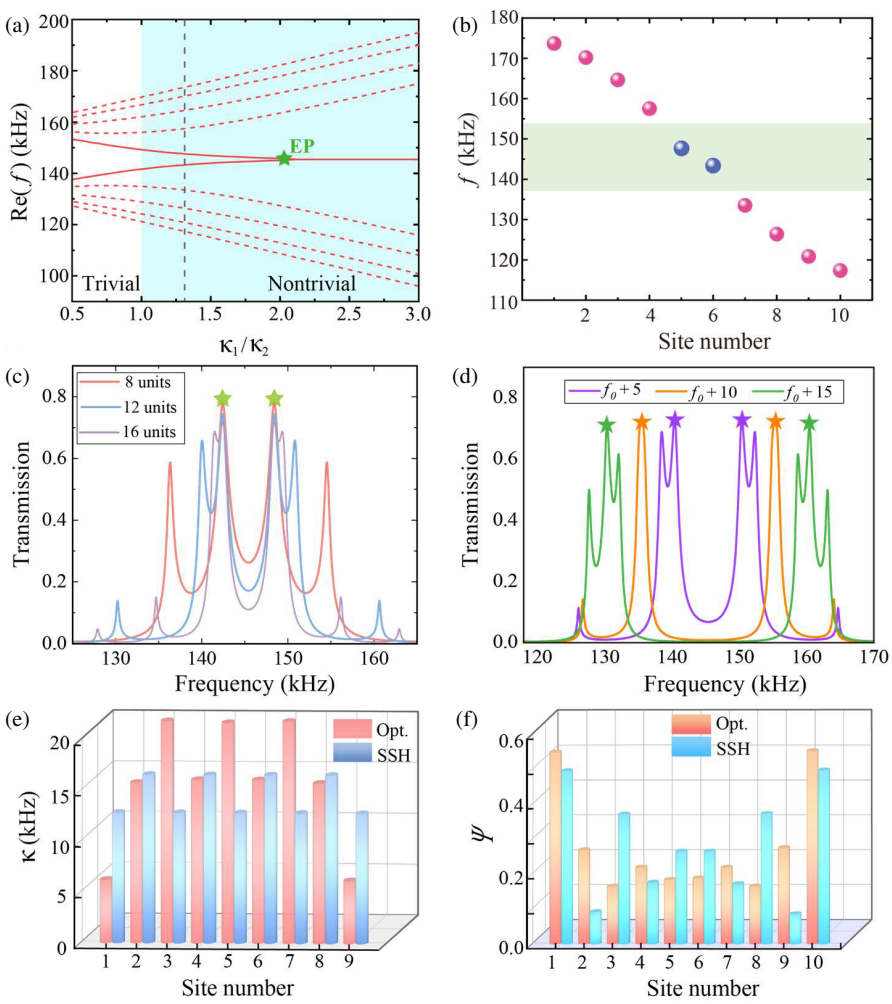

FIGURE 2. The comparison between GDOA results and SSH chains. (a) Real part of the eigenfrequency, with blue and white areas representing the topologically nontrivial phase and the trivial phase, respectively. The red solid and dashed lines indicate edge modes and bulk modes, respectively. The black dashed line marks the experimentally selected $\kappa_1/\kappa_2 = 1.296$. (b) Eigenvalue spectrum of the topological nontrivial SSH chain, with topological modes located within the bandgap (green area). (c) Gradient optimization results for different numbers of oscillator units. (d) Gradient optimization results for different target frequencies. (e) Distribution of coupling strength with respect to the position of resonant coils, with red bars representing the gradient optimized chain and blue bars representing the SSH chain. (f) Distribution of wave functions Ψ, with the same legend as in (e).

on the optimized frequencies around approximately 148.4 kHz (and 142.4 kHz). Due to the symmetry of the system structure, a high transmission point naturally emerges at 142.4 kHz, adjacent to the primary point at 148.4 kHz. Notably, we calculated and compared the frequency values corresponding to the highest transmission rates for each chain: approximately 142.4 kHz for the optimized chain, approximately 141.3 kHz for the SSH chain and 143.3 kHz for the uniform chain.

Next, we delve into the impedance matching analysis of these three types of chains from the perspective of circuit theory. Initially, we set the resistance on the load side to 50 Ω as a benchmark. Subsequently, we calculate the mapped impedance Z_{ref} and input impedance Z_{in}. In this process, the closer the input impedance is to the ideal state (the real part of the resistor is 50 Ω, and the imaginary part of the reactive impedance is 0 Ω), the better the impedance matching is, which subsequently leads to a significant enhancement in the system's transfer efficiency.

Based on Kirchhoff's laws:

$$
\begin{aligned}
&I_{10}\left(i\omega L_{10}+\frac{1}{i\omega C_{10}}\right)-i\omega M_9 I_9+I_{10}R_S=0;\\
&Z_{ref9}=\frac{-i\omega M_9 I_{10}}{I_9};\quad M_9=\frac{2L_9\kappa_9}{\omega};\\
&Z_{ref8}=\frac{-i\omega M_8 I_9}{I_8};\quad M_8=\frac{2L_8\kappa_8}{\omega};\\
&\qquad\ldots\\
&Z_{ref1}=\frac{-i\omega M_1 I_2}{I_1};\quad M_1=\frac{2L_1\kappa_1}{\omega};\\
&Z_{in1}=Z_{ref1}+\frac{1}{i\omega C_1}+i\omega L_1;
\end{aligned}
\tag{7}
$$

where $C_1 = C_2 = \ldots = C_{10}$, $L_1 = L_2 = \ldots = L_{10}$.

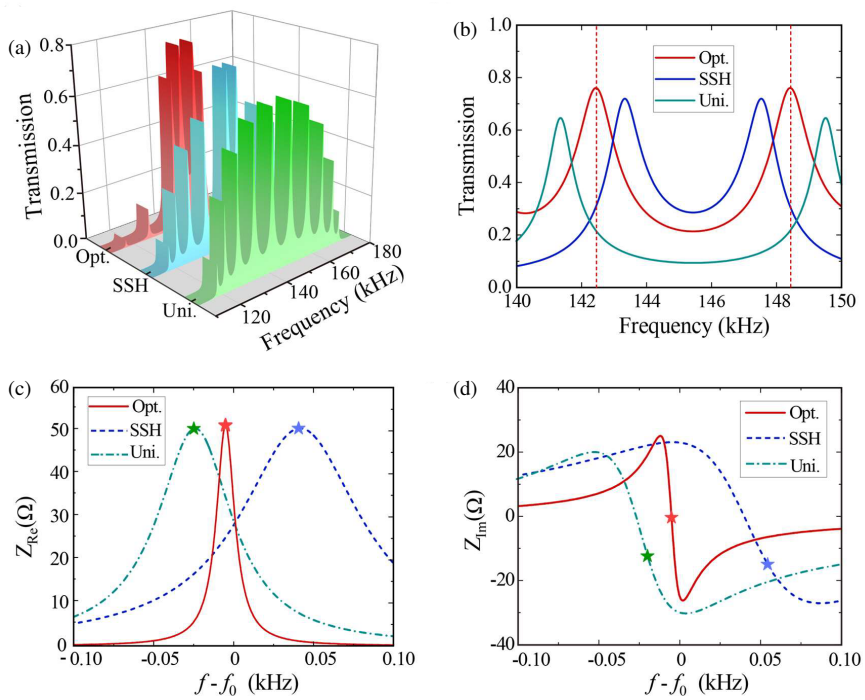

FIGURE 3. Calculated transmission and impedance of three chains. (a) Theoretical calculations have been conducted on the relationship between transmission and frequency for optimized chains (red), SSH chains (blue), and uniform chains (green). (b) The transmission of the three chains near the operating frequency. (c) The real part and (d) imaginary part of their impedances. The pentagrams mark the frequency corresponding to the highest transmission.

The real and imaginary parts of the input impedance for the three types of chains are presented in Figs. 3(c) and 3(d). The red solid line, blue dashed line, and green dashed line depict the impedance characteristics of the optimized chain, SSH chain, and uniform chain, respectively. The pentagram markers indicate the positions with the highest transmission rates on each line. It is evident from the figures that the optimized chain exhibits the best impedance matching effect, followed by the SSH chain, while the uniform chain shows the poorest matching effect. This clear trend is consistent with the calculation results based on CMT presented in Figs. 3(a) and 3(b).

We have successfully verified the theoretical transmission results through experiments. The experimental setup, where two non-resonant coils (Tx and Rx) are connected to the two ports of the vector network analyzer (VNA, SIGLENT SNA5084X), is shown in Fig. 4(a). In this experiment, we employed three types of one-dimensional dimer chains, each consisting of 10 identical sub-wavelength resonant coils carefully constructed. These coils were uniformly wound on circular acrylic plates and equipped with a load capacitance of 5.15 nF. The coils had a diameter of 12 cm, featuring a double-layer winding design with a total of 20 turns, and the inductance value was stable at approximately 222.5 μH, with a resonant frequency close to 145.4 kHz. The non-resonant coils serving as transmitters and receivers were not equipped with load capacitances and had the same diameter of 12 cm, a single-layer winding of 20 turns, and inductance value of 110 μH. The photos of the enlarged resonant coil (right) and non-resonant coil (left) are shown in Fig. 4(b). Notably, we ensured that the total length of the three chains (the distance from the first resonant coil to the tenth resonant coil) was consistently 27 cm, guaranteeing the same transmission distance across all three chains.

Utilizing Vector Network Analyzer (VNA), we connected two non-resonant coils to its ports to assess the transmission of three distinct chains. The experimental outcomes are presented in Fig. 4(c), showcasing the transmission of the optimized, uniform, and SSH chains, which are in agreement with our theoretical predictions (detailed experimental spectral data can be found in the Supplementary Information E [43]). Additionally, Fig. 4(d) unveils the transmission trends of these three chains across varying gain g and loss γ. Notably, across the entire test range, the optimized chain (experimental data marked with green dots) exhibits significantly better transmission performance than the SSH chain and uniform chain. The scalability and generality of the GDOA approach are validated through additional experiments on extended systems with 12 and 14 resonators, as detailed in the Supplementary Information F [43]. In all configurations, GDOA consistently achieves high transmittance (> 0.6) at the target frequency of 142.4 kHz, showing minimal sensitivity to chain length variations. These results confirm the method's robustness and adaptability across different system scales, effectively addressing the limitations of fixed-size assumptions. This scalability underscores the algorithm's strong potential for practical, flexible, and efficient long-range WPT applications.

In finite topological systems, zero modes, as topological edge states, often deviate from the exact zero-energy state in finite Hermitian lattices due to the coupling between these edge states. This coupling inevitably weakens topological protection and reduces the robustness of SSH chains [45, 46]. Neverthe-

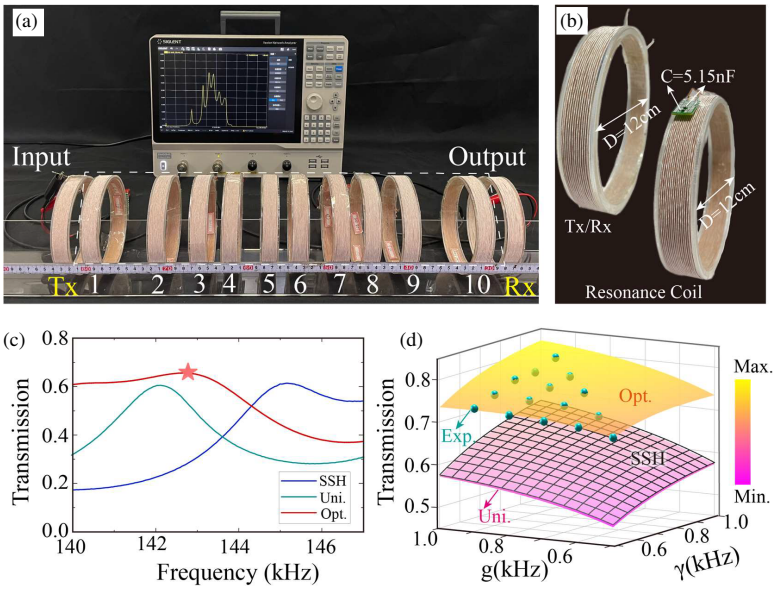

FIGURE 4. Experimental comparison of transmission and robustness of three types of chains. (a) The photo of the experimental setup consists of 10 resonant coils, a left non-resonant source coil, a right non-resonant receiver coil, and a VNA. (b) Photos of the enlarged resonant coil (right) and non-resonant coil (left). (c) Experimental measured transmission of the three chains, where the pentagram represents the maximum transmission of the optimized chain at the operating frequency. (d) The relationship diagram between transmission, gain, and loss rate of three types of chains. The green spheres correspond to the experimental results.

TABLE 1. Comparison of parameters and performance with other literature.

Ref.	Number of coils	The resonance order of the system	Coil radius (cm)	Distance to diameter ratio	Transmission range	Transmission efficiency (η)	Transmission capability[a]	Not limited by resonant frequency	Robust to structural fluctuations	Robust to transmission distance	Overall robustness[b]
[2]	2	2	30	8	Mid-far	0.4	B	Yes	No	No	B
[20]	2	2	29	2.1	Mid-far	0.9	A	Yes	No	Yes	A
[12]	2	3	4.3	4	Mid-far	0.9	A	No	No	Yes	B
[17]	3	3	15	2	Mid-far	0.8	A−	No	No	Yes	B
[13]	11	11	15.5	11.6	Far	0.5	A−	Yes	No	No	B
[24]	10	10	4	10.5	Far	0.6	A	No	Yes	No	B
[23]	16	16	2.6	9.6	Far	0.1	B−	No	Yes	No	B
[25]	16	16	2.6	9.6	Far	0.1	B−	Yes	Yes	No	A
This work	10	10	6	11.8	Far	0.64	A	Yes	Yes	Yes	A+

Note: [a] Transmission capability grades: A: Far distance and $\eta \geq 0.6$, or Mid-far distance and $\eta \geq 0.8$; A−: Far distance and $0.5 \ll \eta < 0.6$, or Mid-far distance and $0.8 \ll \eta < 0.9$; B: Mid-far distance and $0.4 \ll \eta < 0.5$; B−: Far distance and $0.1 \ll \eta < 0.2$.
[b] Overall robustness grades: A+: All criteria "Yes"; A: Two criteria are "Yes"; B: One criterion is "Yes."

less, these localized modes are more stable than the normal bulk states [45, 46]. Therefore, we further compared the robustness of the three chains. The magnitude of disorder perturbations was determined by the product of the perturbation intensity and a random number ranging from 0 to 1, with disorder introduced by adjusting the coupling coefficients. We further experimentally investigated the robustness of these three chains under different perturbation intensities. We display a comparison of the transmission rates of the three chains under different perturbation intensities. Specifically, Fig. 5 illustrates the comparison results at a perturbation intensity of 30%. The theoretical calculations here were based on averages from 10000 random perturbation instances as a reference benchmark. (Detailed data can be found in the Supplementary Information E [43]). The experimental results clearly demonstrate that the optimized chain not only exhibits higher transmission efficiency, but also inherits the robustness of the SSH model to structural perturbation immunity. The robustness of the optimized chain stems from its topological characteristics. In finite SSH-like systems, edge states are protected against perturbations that preserve the system's symmetry. Finally, we compared the system parameters and performance of our work with those reported in other stud-

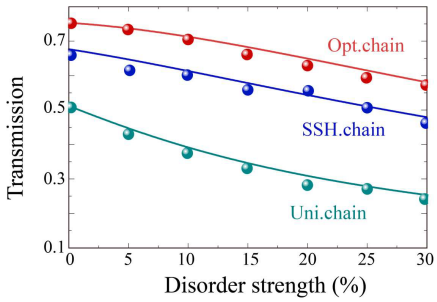

FIGURE 5. The transmission of three types of chains varies with the intensity of disorder disturbance. The calculated and measured results are marked by the solid lines and dots, respectively.

ies, as summarized in Table 1. To provide a more intuitive representation of the performance differences among various systems, we use letter grades: A+ denotes the best performance, A the excellent performance, A− the slightly weaker performance, and so on. As shown in the table, our system demonstrates the highest overall robustness.

3. CONCLUSION

In summary, we have optimized a long-range multi-relay coil WPT system using the GDOA, innovatively proposing a novel WPT scheme that is both efficient and robust. Through dual verifications by CMT and circuit theory, we have proven that the optimized transmission significantly surpasses that of SSH chains and uniform chains, which has been further confirmed through experiments. Furthermore, we have conducted a thorough analysis of the stability performance of uniform chains, SSH chains, and optimized chains at their respective optimal operating frequencies. The results indicate that the optimized chain system exhibits the strongest anti-interference capability against perturbations in position-dependent coupling strength, implying higher stability when being faced with disturbances such as transmission distance variations. In industrial and daily applications, there is an urgent demand for long-distance, high-stability, and efficient chained WPT technology, particularly in areas such as the long arms of mobile machinery, high-voltage power transmission detection, and feedback devices [47, 48]. Machine learning not only helps to accurately identify topological phases [49, 50], but also significantly improves the technical performance of one-dimensional systems. Considering that most power supplies in real-life scenarios have fixed output frequencies, we have optimized the chained WPT using the GDOA, enabling it to achieve high transfer efficiency and demonstrate strong adaptability to changes in power supply output frequency. Meanwhile, in the supplementary materials, we have detailed the exceptional flexibility of the GDOA in optimizing frequency and the number of oscillators, which is highly attractive for practical industrial applications.

ACKNOWLEDGEMENT

This work is supported by the National Key R&D Program of China (Nos. 2023YFA1407600 and 2021YFA1400602), the National Natural Science Foundation of China (Nos. 12104342, 12374294, and 52477014), the Interdisciplinary key project of Tongji University (No. 2023-1-ZD-02), the Shanghai Science and Technology Commission Project (No. 2021SHZDZX0100), and the Chenguang Program of Shanghai (No. 21CGA22).

REFERENCES

[1] Tesla, N., "Apparatus for transmitting electrical energy," U.S. Patent, US1119732A, 1914.

[2] Kurs, A., A. Karalis, R. Moffatt, J. D. Joannopoulos, P. Fisher, and M. Soljačić, "Wireless power transfer via strongly coupled magnetic resonances," *Science*, Vol. 317, No. 5834, 83–86, 2007.

[3] Ahn, D. and S. Hong, "Wireless power transmission with self-regulated output voltage for biomedical implant," *IEEE Transactions on Industrial Electronics*, Vol. 61, No. 5, 2225–2235, 2013.

[4] Kim, S., J. S. Ho, and A. S. Y. Poon, "Midfield wireless powering of subwavelength autonomous devices," *Physical Review Letters*, Vol. 110, No. 20, 203905, 2013.

[5] Ho, J. S., A. J. Yeh, E. Neofytou, S. Kim, Y. Tanabe, B. Patlolla, R. E. Beygui, and A. S. Y. Poon, "Wireless power transfer to deep-tissue microimplants," *Proceedings of the National Academy of Sciences*, Vol. 111, No. 22, 7974–7979, 2014.

[6] Mei, H. and P. P. Irazoqui, "Miniaturizing wireless implants," *Nature Biotechnology*, Vol. 32, No. 10, 1008–1010, 2014.

[7] Lu, X., D. Niyato, P. Wang, D. I. Kim, and Z. Han, "Wireless charger networking for mobile devices: Fundamentals, standards, and applications," *IEEE Wireless Communications*, Vol. 22, No. 2, 126–135, 2015.

[8] Lerosey, G., "Wireless power on the move," *Nature*, Vol. 546, No. 7658, 354–355, 2017.

[9] Sample, A. P., D. T. Meyer, and J. R. Smith, "Analysis, experimental results, and range adaptation of magnetically coupled resonators for wireless power transfer," *IEEE Transactions on Industrial Electronics*, Vol. 58, No. 2, 544–554, 2010.

[10] Miao, Z., D. Liu, and C. Gong, "Efficiency enhancement for an inductive wireless power transfer system by optimizing the impedance matching networks," *IEEE Transactions on Biomedical Circuits and Systems*, Vol. 11, No. 5, 1160–1170, 2017.

[11] Li, H., J. Li, K. Wang, W. Chen, and X. Yang, "A maximum efficiency point tracking control scheme for wireless power transfer systems using magnetic resonant coupling," *IEEE Transactions on Power Electronics*, Vol. 30, No. 7, 3998–4008, 2014.

[12] Guo, Z., F. Yang, H. Zhang, X. Wu, Q. Wu, K. Zhu, J. Jiang, H. Jiang, Y. Yang, Y. Li, and H. Chen, "Level pinning of anti-PT-symmetric circuits for efficient wireless power transfer," *National Science Review*, Vol. 11, No. 1, nwad172, 2024.

[13] Zhong, W., C. K. Lee, and S. Y. R. Hui, "General analysis on the use of Tesla's resonators in domino forms for wireless power transfer," *IEEE Transactions on Industrial Electronics*, Vol. 60, No. 1, 261–270, 2011.

[14] Kim, J. W., H.-C. Son, K.-H. Kim, and Y.-J. Park, "Efficiency analysis of magnetic resonance wireless power transfer with intermediate resonant coil," *IEEE Antennas and Wireless Propagation Letters*, Vol. 10, 389–392, 2011.

[15] Saha, C., I. Anya, C. Alexandru, and R. Jinks, "Wireless power transfer using relay resonators," *Applied Physics Letters*, Vol. 112, No. 26, 263902, 2018.

[16] Sakhdari, M., M. Hajizadegan, and P.-Y. Chen, "Robust extended-range wireless power transfer using a higher-order PT-symmetric platform," *Physical Review Research*, Vol. 2, No. 1, 013152, 2020.

[17] Guo, Z., J. Jiang, X. Wu, H. Zhang, S. Hu, Y. Wang, Y. Li, Y. Yang, and H. Chen, "Rotation manipulation of high-order PT-symmetry for robust wireless power transfer," *Fundamental Research*, Vol. 11, 10, 2023.

[18] Song, M., P. Jayathurathnage, E. Zanganeh, M. Krasikova, P. Smirnov, P. Belov, P. Kapitanova, C. Simovski, S. Tretyakov, and A. Krasnok, "Wireless power transfer based on novel physical concepts," *Nature Electronics*, Vol. 4, No. 10, 707–716, 2021.

[19] Zeng, C., Z. Guo, K. Zhu, C. Fan, G. Li, J. Jiang, Y. Li, H. Jiang, Y. Yang, Y. Sun, and H. Chen, "Efficient and stable wireless power transfer based on the non-Hermitian physics," *Chinese Physics B*, Vol. 31, No. 1, 010307, 2022.

[20] Assawaworrarit, S., X. Yu, and S. Fan, "Robust wireless power transfer using a nonlinear parity-time-symmetric circuit," *Nature*, Vol. 546, No. 7658, 387–390, 2017.

[21] Zhou, J., B. Zhang, W. Xiao, D. Qiu, and Y. Chen, "Nonlinear parity-time-symmetric model for constant efficiency wireless power transfer: Application to a drone-in-flight wireless charging platform," *IEEE Transactions on Industrial Electronics*, Vol. 66, No. 5, 4097–4107, 2018.

[22] Feis, J., C. J. Stevens, and E. Shamonina, "Wireless power transfer through asymmetric topological edge states in diatomic chains of coupled meta-atoms," *Applied Physics Letters*, Vol. 117, No. 13, 134106, 2020.

[23] Song, J., F. Yang, Z. Guo, X. Wu, K. Zhu, J. Jiang, Y. Sun, Y. Li, H. Jiang, and H. Chen, "Wireless power transfer via topological modes in dimer chains," *Physical Review Applied*, Vol. 15, No. 1, 014009, 2021.

[24] Zhang, L., Y. Yang, Z. Jiang, Q. Chen, Q. Yan, Z. Wu, B. Zhang, J. Huangfu, and H. Chen, "Demonstration of topological wireless power transfer," *Science Bulletin*, Vol. 66, No. 10, 974–980, 2021.

[25] Yang, F., J. Song, Z. Guo, X. Wu, K. Zhu, J. Jiang, Y. Sun, H. Jiang, Y. Li, and H. Chen, "Actively controlled asymmetric edge states for directional wireless power transfer," *Optics Express*, Vol. 29, No. 5, 7844–7857, 2021.

[26] Zhang, H., Z. Guo, Y. Li, Y. Yang, Y. Chen, and H. Chen, "A universal non-hermitian platform for bound state in the continuum enhanced wireless power transfer," *Frontiers of Physics*, Vol. 19, No. 4, 43209, 2024.

[27] Ma, W., Z. Liu, Z. A. Kudyshev, A. Boltasseva, W. Cai, and Y. Liu, "Deep learning for the design of photonic structures," *Nature Photonics*, Vol. 15, No. 2, 77–90, 2021.

[28] Genty, G., L. Salmela, J. M. Dudley, D. Brunner, A. Kokhanovskiy, S. Kobtsev, and S. K. Turitsyn, "Machine learning and applications in ultrafast photonics," *Nature Photonics*, Vol. 15, No. 2, 91–101, 2021.

[29] Nadell, C. C., B. Huang, J. M. Malof, and W. J. Padilla, "Deep learning for accelerated all-dielectric metasurface design," *Optics Express*, Vol. 27, No. 20, 27 523–27 535, 2019.

[30] Wu, Y., Z. Meng, K. Wen, C. Mi, J. Zhang, and H. Zhai, "Active learning approach to optimization of experimental control," *Chinese Physics Letters*, Vol. 37, No. 10, 103201, 2020.

[31] Henson, B. M., D. K. Shin, K. F. Thomas, J. A. Ross, M. R. Hush, S. S. Hodgman, and A. G. Truscott, "Approaching the adiabatic timescale with machine learning," *Proceedings of the National Academy of Sciences*, Vol. 115, No. 52, 13 216–13 221, 2018.

[32] Nakamura, I., A. Kanemura, T. Nakaso, R. Yamamoto, and T. Fukuhara, "Non-standard trajectories found by machine learning for evaporative cooling of 87Rb atoms," *Optics Express*, Vol. 27, No. 15, 20 435–20 443, 2019.

[33] Bukov, M., A. G. R. Day, D. Sels, P. Weinberg, A. Polkovnikov, and P. Mehta, "Reinforcement learning in different phases of quantum control," *Physical Review X*, Vol. 8, No. 3, 031086, 2018.

[34] Guo, S.-F., F. Chen, Q. Liu, M. Xue, J.-J. Chen, J.-H. Cao, T.-W. Mao, M. K. Tey, and L. You, "Faster state preparation across quantum phase transition assisted by reinforcement learning," *Physical Review Letters*, Vol. 126, No. 6, 060401, 2021.

[35] Lin, J., Z. Y. Lai, and X. Li, "Quantum adiabatic algorithm design using reinforcement learning," *Physical Review A*, Vol. 101, No. 5, 052327, 2020.

[36] Schiffer, B. F., J. Tura, and J. I. Cirac, "Adiabatic spectroscopy and a variational quantum adiabatic algorithm," *PRX Quantum*, Vol. 3, No. 2, 020347, 2022.

[37] Mukherjee, R., H. Xie, and F. Mintert, "Bayesian optimal control of Greenberger-Horne-Zeilinger states in Rydberg lattices," *Physical Review Letters*, Vol. 125, No. 20, 203603, 2020.

[38] Choi, B.-G. and Y.-S. Kim, "New structure design of ferrite cores for wireless electric vehicle charging by machine learning," *IEEE Transactions on Industrial Electronics*, Vol. 68, No. 12, 12 162–12 172, 2021.

[39] Rahulkumar, J. and R. Narayanamoorthi, "Delta and inverse delta coupler optimization using machine learning for wireless power transfer electric vehicle charging application," *IEEE Transactions on Power Electronics*, Vol. 40, No. 1, 2556–2568, 2025.

[40] Liu, X., J. Chao, C. Rong, Z. Liao, and C. Xia, "Compatibility and performance improvement of the WPT systems based on Q-learning algorithm," *IEEE Transactions on Power Electronics*, Vol. 39, No. 8, 10 582–10 593, 2024.

[41] Srivastava, V. K., A. Ahmad, and A. Sharma, "A machine learning assisted localization and magnetic field forming for wireless powering of biomedical implant devices," *IEEE Transactions on Antennas and Propagation*, Vol. 72, No. 11, 8590–8599, 2024.

[42] Magann, A. B., K. M. Rudinger, M. D. Grace, and M. Sarovar, "Feedback-based quantum optimization," *Physical Review Letters*, Vol. 129, No. 25, 250502, 2022.

[43] See Supplemental Material at *** for detailed derivations of GDOA validation, the imaginary parts of the eigenfrequencies in SSH, and more experimental results.

[44] Fan, S., W. Suh, and J. D. Joannopoulos, "Temporal coupled-mode theory for the Fano resonance in optical resonators," *Journal of the Optical Society of America A*, Vol. 20, No. 3, 569–572, 2003.

[45] Guo, Z., T. Zhang, J. Song, H. Jiang, and H. Chen, "Sensitivity of topological edge states in a non-Hermitian dimer chain," *Photonics Research*, Vol. 9, No. 4, 574–582, 2021.

[46] Song, W., W. Sun, C. Chen, Q. Song, S. Xiao, S. Zhu, and T. Li, "Breakup and recovery of topological zero modes in finite non-Hermitian optical lattices," *Physical Review Letters*, Vol. 123, No. 16, 165701, 2019.

[47] Shiba, K., A. Morimasa, and H. Hirano, "Design and development of low-loss transformer for powering small implantable medical devices," *IEEE Transactions on Biomedical Circuits and Systems*, Vol. 4, No. 2, 77–85, 2010.

[48] Beh, T. C., M. Kato, T. Imura, S. Oh, and Y. Hori, "Automated impedance matching system for robust wireless power transfer via magnetic resonance coupling," *IEEE Transactions on Industrial Electronics*, Vol. 60, No. 9, 3689–3698, 2012.

[49] Long, Y., J. Ren, and H. Chen, "Unsupervised manifold clustering of topological phononics," *Physical Review Letters*, Vol. 124, No. 18, 185501, 2020.

[50] Long, Y. and B. Zhang, "Unsupervised data-driven classification of topological gapped systems with symmetries," *Physical Review Letters*, Vol. 130, No. 3, 036601, 2023.